arXiv:1602.03637v1 [nucl-th] 11 Feb 2016

Asymptotic normalization coefficients for $^7\mathrm{Be} + p \to {}^8\mathrm{B}$ from the peripheral $^7\mathrm{Be}(d,n)^8\mathrm{B}$ reaction and their astrophysical application

O. Tojiboev[1)], R. Yarmukhamedov[1)*], S. V. Artemov[1)], S. B. Sakuta[2)]

February 12, 2016

[1)] *Institute of Nuclear Physics, Tashkent 100214, Uzbekistan*
[2)] *National Research Center "Kurchatov Institute", Moscow 123182, Russia*

Abstract

The proton transfer $^7\mathrm{Be}(d,n)^8\mathrm{B}$ reaction at the energy of 4.5 MeV (c.m.) has been analysed within the modified DWBA. New estimates and their uncertainties are obtained for values of the asymptotic normalization coefficients for $p + {}^7\mathrm{Be} \to {}^8\mathrm{B}$, the astrophysical $S_{17}(0)$ factor and the s-wave p+^{7}Be scattering lengths.

PACS: 25.55.-e;26.35.+c;26.65.+t

I. INTRODUCTION

The radiative capture $^7\mathrm{Be}(p,\gamma)^8\mathrm{B}$ reaction rate given in terms of the extremely-low energy astrophysical S factor is one of the main input data for calculations of the solar-neutrino flux [1–6]. At the stellar temperature $T_6 \sim 15$ K, this rate determines how much the ^{7}Be and ^{8}B branches of the *pp* chain contribute to the hydrogen burning. In the standard solar model, the predicted flux of neutrinos is determined by the relation [1]

$$\phi_\nu \sim \tilde{S}_{11}^{-2.5} \tilde{S_{33}}^{-0.3} \tilde{S_{34}}^{0.8} [1 + 3.47 \tilde{S_{17}} \tilde{\tau}_{e7}^{-1}]. \quad (1)$$

Here $\tilde{S_{ij}} = S_{ij}(E)/S_{ij}(0)$ and $\tilde{\tau_{e7}} = \tau_{e7}(E)/\tau_{e7}(0)$, where $S_{ij}(E)$ is the extremely-low energy astrophysical S factor for the reactions of the *pp* chain induced by collisions of the nuclei with mass numbers i and j, $\tau_{e7}(E)$ is the ^{7}Be lifetime with respect to the electron capture $^7\mathrm{Be} + e^- \to {}^7\mathrm{Li} + \nu_e$ reaction and E is the relative kinetic energy of the colliding particles. It is seen that the flux of neutrinos depends noticeably on the β-decay of ^{8}B determined in turn by

*Corresponding author, E-mail: rakhim@inp.uz

the accuracy of the astrophysical S factors of the ^{7}Be(p,γ)^{8}B reaction at so far experimentally inaccessible solar energies ($E \lesssim 25$ keV), including E=0.

It is known that the uncertainty in extrapolation of the astrophysical S factors to the Gamow energy E_G=18 keV obtained at the stellar temperature T_6=15 K (Sun) [7] affects significantly the predicted flux of solar ^{8}B neutrinos [6, 8].

Despite the impressive improvements in our understanding the nuclear-astrophysical ^{7}Be(p, γ)^{8}B reaction made in a period of ten consecutive years, some ambiguities connected with both the extrapolation of the astrophysical S factors to the solar energy region and the theoretical prediction for $S_{17}(E)$ still exist and can influence the prediction of the standard solar model [6]. For example, the analysis of the precisely measured astrophysical S factors for the ^{7}Be(p, γ)^{8}B reaction and their extrapolation performed by different authors from the observed energy regions to extremely low experimentally inaccessible energies gives values of $S_{17}(0)$ with a spread exceeding noticeably the experimental ones (see the recent reviews [8, 9] and references therein as well as Ref. [10]). As regards the theoretical microscopic calculations of $S_{17}(0)$, they also show considerable spread connected with the method used (see, for example, Refs. [11–13] and the available references therein). It should be noted that a considerable sensitivity of the calculated value of $S_{17}(0)$ is observed in [11–13] to the used effective nucleon-nucleon potential. Moreover, as it is evident from these works, a correlation has been revealed between the asymptotic normalization coefficients (ANC) calculated for $p + {}^7\mathrm{Be} \to {}^8\mathrm{B}$, which determine the amplitude of the tail of the radial ^{8}B nucleus bound wave function in the (^{7}Be+p)-channel [14], and the calculated $S_{17}(0)$.

Taking into account this fact, in the last years several works have been performed to determine the ANC for $p + {}^7\mathrm{Be} \to {}^8\mathrm{B}$ and the $S_{17}(0)$ with an accuracy as high as possible. In [10], the "indirectly determined" value of ANCs for ${}^7\mathrm{Be} + p \to {}^8\mathrm{B}$ were obtained by means of the analysis of the precisely measured experimental astrophysical S factors ($S_{17}^{exp}(E)$) performed within the modified two-body potential approach (MTBPA) [15] where $S_{17}(E)$ for the direct radiative capture ^{7}Be(p, γ)^{8}B reaction is expressed in terms of ANC for $p + {}^7\mathrm{Be} \to {}^8\mathrm{B}$. Then the derived ANC was used for extrapolation of the corresponding astrophysical S factors to solar energies. In [16] (see also [17, 18]), the ANC values for $p + {}^7\mathrm{Be} \to {}^8\mathrm{B}$ were obtained from analysis of the peripheral proton transfer ^{10}B(^{7}Be,^{8}B)^{9}Be and ^{14}N(^{7}Be,^{8}B)^{13}C reactions. The analysis was performed within the modified DWBA restricting by the first order of the perturbation theory over the Coulomb polarization potential (ΔV_f^C) in the transition operator and assuming that its contribution to the total transition operator is small. But, the ANC values proposed in [16] may not have sufficient accuracy because of the aforementioned assumption made for the transition operators [19, 20]. Nevertheless, in [16] the obtained ANC values were then used for the estimation of $S_{17}(0)$, which also differs noticeably from that recommended in [8, 10, 21]. As is noted in [10, 20], one of the main reasons of the observed discrepancy is connected with underestimated values of the ANCs suggested in [16] as compared with that obtained in [10, 20].

This disagreement initiated a number of the new measurements of other kinds of peripheral nuclear processes to obtain an additional information about the ANC values for ${}^7\mathrm{Be} + p \to {}^8\mathrm{B}$ and their astrophysical application. Particularity, the analysis of the experimental differential cross sections for the peripheral proton transfer ^{7}Be(d,n)^{8}B reaction, measured in inverse kine-

matics at the energies 5.8 [22] and 4.5 MeV [23] in the center of mass system (denoted by E_i everywhere below), was performed in [22, 24] and [23], respectively. In [22, 23] and [24], the analysis was carried out within the standard DWBA and the three-body approach with the effects of breakup of the deuteron in the field of the target treated by means of continuum-discretized coupled-channel method (CDCCM). There the calculated cross sections are expressed in terms of the spectroscopic factors for the ^{8}B nucleus in the (^{7}Be + p)-configuration. Besides, in [22], for the transferred proton only the $1p_{3/2}$ configuration was only taken into account. However, the extracted in [22, 24] and [23] spectroscopic factors, used for obtaining the ANC values, may not be accurate enough. This is connected with the fact that the calculated single particle cross sections, as will be shown below, become very sensitive to the adopted values of the geometric parameters of the Woods-Saxon potential used for calculation of the bound ^{8}B[=(^{7}Be+p)] state wave function [25]. The results of the analysis of the experimental differential cross sections [22] of the ^{7}Be(d,n)^{8}B reaction obtained in [26] within the modified DWBA [27–29], where the differential cross section is expressed in terms of the ANC but not in terms of the spectroscopic factors, should also be noted. In [26], the ANC values for $^7\mathrm{Be}+p \to {}^8$B were obtained by using the optical potentials recommended in [22] for the entrance and exit channels, but contribution of the compound nucleus evaluated in [22] and the coupled channels effects were not taken into account. So, it should be noted that, firstly, the experimental data of [22] in the main peak region of the angular distribution have fairly large errors not only in the absolute values of the differential cross sections but also in the angle resolution. Secondly, as is shown in [23], calculations with the optical parameters of [22] for the entrance channel, which are also used in [26], reproduce the corresponding experimental scattering data only in a narrow angular interval of the forward hemisphere. Therefore, the ANC values of [26] also may not have enough accuracy for the astrophysical application. In this connection, it is of great interest to apply the modified DWBA for the analysis of the experimental data of the ^{7}Be(d,n)^{8}B reaction measured in [23] since they are more peripheral and more precise than the data of [22].

In the present work, the reanalysis of the experimental differential cross sections [23] for the ^{7}Be(d,n)^{8}B reaction at energy E_i=4.5 MeV is performed within the modified DWBA [27–29] to obtain the "indirectly determined" values of the ANC for $^7\mathrm{Be}+p \to {}^8$B, which were then used for estimation of the $S_{17}(0)$. Here, we quantitatively show that the ^{7}Be(d,n)^{8}B reaction measured in [23] is practically peripheral in the main peak region of the angular distribution. Therefore, the ambiguities, which are connected both with the variation of the geometric parameters (radius r_o, diffuseness a) of the Woods-Saxon potential used for calculating of the bound state wave functions and with choice of a set of the optical parameters, are reduced to the physically acceptable limit, being within the errors of the analyzed experimental differential cross sections.

II. ANALYSIS OF THE ^{7}Be$(d,n)^8$B REACTION

A. The basic formulas of the modified DWBA

Here we present only the main idea and the essential formulas of the MDWBA [28, 29] specialized for the ^{7}Be(d,n)^{8}B reaction.

Let us write $l_B(j_B)$ for the orbital (total) angular momentum of the proton in the ^{8}B nucleus and $l_d(j_d)$ for the proton in the deuteron. For the ^{7}Be(d,n)^{8}B reaction the value of l_B is taken to be equal to 1 and the values of j_B are taken to be equal to 1/2 and 3/2, while the values l_d and j_d are taken equal to 0 and 1/2 for s-wave and to 2 and 3/2 for d-wave, respectively.

The main contribution to the full transition operator in the amplitude (at least near the main peak region in the angular distribution) comes from the proton-neutron nuclear V_{np}^N potential [19, 30, 31] since ΔV_f^C=0 in the full transition operator because of the presence of a neutron in the final state. Then the single particle DWBA cross section can be calculated within the finite range DWBA in the "post"-approximation with the DWUCK5 code. But if the reaction under consideration is peripheral, the influence of the ambiguity of the optical model parameters on the calculated single particle DWBA cross section should be small, at least not exceeding the experimental errors. In this case, the largest uncertainty in the single particle DWBA cross section comes from its strong dependence on the geometric parameters (radius r_0 and diffuseness a) of the Woods–Saxon potential used for calculating the radial wave function of the single-particle ^{8}B[=(^{7}Be + p)] bound state wave function. It is known that this dependence enters the single particle DWBA cross section mainly through the corresponding single-particle ANC [25]. It will be demonstrated below that the reaction ^{7}Be(d,n)^{8}B at E_i=4.5 MeV is peripheral, so the single-particle ANCs for the shell model bound wave functions of the residual nucleus 8B, entering the calculated single particle DWBA cross section, are the free parameters.

Only s wave is taken into account for the deuteron wave function in our calculations. This approximation is justified by the fact that the reaction under consideration has the peripheral character at least in the main peak region of the angular distribution. Therefore, in this angle region the dominant contribution to the DWBA cross sections comes from the surface and outer regions of the colliding nuclei. In this interaction region, contribution of the d wave component to the deuteron wave function is strongly suppressed since the amplitude of its "tail" determined by the corresponding ANC of the d wave is very small ($\sim$10^{-2} fm$^{-1/2}$) as compared to that for the s wave [14, 32].

Then, according to [27–29], within the modified DWBA, we can write the differential cross section in the form

$$\frac{d\sigma}{d\Omega} = C^2_{B;\,3/2}[\mathcal{R}_{3/2}(E_i,\theta;\, b_{B;3/2}) + \lambda\mathcal{R}_{1/2}(E_i,\theta;\, b_{B;1/2})], \tag{2}$$

$$\mathcal{R}_{j_B}(E_i,\theta;\, b_{B;\,j_B}) = \left(\frac{C_{d;\,1/2}}{b_{d;\,1/2}}\right)^2 \frac{\sigma^{\rm DW}_{j_B}(E_i,\theta;\, b_{B;\,j_B})}{b^2_{B;\,j_B}}, \tag{3}$$

where $C_{d;\,j_d}$ and $C_{B;\,j_B}$ are the ANCs for p+n $\to$ d and ^{7}Be+p $\to$ ^{8}B; E_i is the relative kinetic energy of the colliding particles; θ is the scattering angle in c.m.s. and $\lambda = (C_{B;\,1/2}/C_{B:\,3/2})^2$=0.125 [16, 33]. In Eqs. (2) and (3), $b_{B;\,j_B}$ is the single particle ANCs for the shell model wave function for the bound (^{7}Be + p) state, which determine the amplitude of its tail [14]; $b_{d;\,j_d}$ is the amplitude of the tail of the s wave deuteron wave function of relative motion of the neutron and proton in the deuteron (j_d=1/2); $\sigma^{\rm DW}_{j_B}(E_i,\theta;\, b_{B;\,j_B})$ is the single-particle DWBA cross section. For independent testing, the single-particle DWBA cross section has also been calculated using the LOLA code [31] restricted only by the first order perturbation term of over ΔV_f^C in the

transition operator. Both calculations gave the same results since ΔV_f^C=0. In (2), the ANC $C_{B;\,j_B}$, the single particle ANCs $b_{B;\,j_B}$ (j_B=1/2 and 3/2) and the parameter $b_{d;\,1/2}$ are unknown, whereas the values of the ANC for $p+n \to d$ ($C_{d;\,1/2}$) and λ are known [14, 16, 32]. Nevertheless, the value of the free parameter $b_{d;\,j_d}$ can be determined by similar way as it was done in [17, 18, 28] as the "experimental" ANC value for $p+n \to d$ extracted from the exchange nd and pd scatterings is known with the high accuracy ($C^2_{d;\,1/2}$=0.774±0.018 fm^{-1}) [14, 32]. Besides, this value of the ANC is in excellent agreement with that calculated by different forms of the realistic NN potential where its value was found insensitive to the used form of the NN potential (see [14] for example). This circumstance makes it possible to calculate the s wave of the deuteron wave function by using the Woods-Saxon potential with the geometric parameters chosen to reproduce the aforementioned ANC value of $C_{d;\,1/2}$ and to fix the value of $b_{d;\,1/2}$ at 0.942 fm$^{-1/2}$.

To make the dependence of the $\mathcal{R}_{j_B}(E_i,\theta;\,b_{B;\,j_B})$ function on $b_{B;\,j_B}$ more transparent, we have used the zero-range version of DWBA for the V^N_{np} potential with fixed optical model parameters in the initial and final states. Note that this consideration is also valid for the finite range of DWBA. In the radial integral for the matrix element [30] in the $\mathcal{R}_{j_B}(E_i,\theta;\,b_{B;\,j_B})$ function we split the space of interaction of the colliding particles in two parts separated by the channel radius R_{ch} [25]: the interior part ($0\leq R \leq R_{ch}$), where nuclear forces between the colliding nuclei are important, and the exterior part ($R_{ch} \leq R < \infty$), where the interaction between the colliding nuclei is governed by Coulomb forces only. The exterior part of the radial integral for the matrix element in the $\mathcal{R}_{j_B}(E_i,\theta;\,b_{B;\,j_B})$ function does not contain explicitly the free parameter $b_{B;\,j_B}$, since for $R > R_{ch}$ the bound [(^{7}Be + p)] state wave function $\varphi_{B;\,j_B}(R)$[=$\varphi_{B;\,j_B}(R;b_{B;\,j_B})$ [25]] can be approximated by its asymptotic behavior [14]. Consequently, parametrization of the differential cross section in the form (2) allows to fix the contribution from the exterior region in a model independent way, if it is dominant for the peripheral reaction and if the ANCs $C_{B;\,j_B}$ (j_B=1/2 and 3/2) are known. In that case the contribution from the interior part of the radial matrix element to the $\mathcal{R}_{j_B}(E_i,\theta;\,b_{B;\,j_B})$ function, which depends on $b_{B;\,j_B}$ through the fraction $\varphi_{B;\,j_B}(R;b_{B;\,j_B})/b_{B;\,j_B}$ [25, 30], exactly determines the dependence of the $\mathcal{R}_{j_B}(E_i,\theta;\,b_{B;\,j_B})$ function on $b_{B;\,j_B}$. It should be noted that this fraction is convolved with the radial optical wave functions in the initial and final states in the integrand of the radial integral for the interior part of the matrix element. The contribution from the interior part to the $d\sigma/d\Omega$ cross section is determined by the free parameters $b_{B;\,j_B}$ and the spectroscopic factors $Z_{B;\,j_B}$ through the product of $Z^{1/2}_{B;\,j_B}\varphi_{B;\,j_B}(R;b_{B;\,j_B})$, which is really model dependent due to the unknown free parameters $b_{B;\,j_B}$. One notes that the spectroscopic factor ($Z^{1/2}_{B;\,j_B}$), which is a norm of the radial overlap function of the bound state ^{8}B wave function in the (^{7}Be+p)-channel, is related to the ANC $C_{B;\,j_B}$ by the equation [14]

$$C_{B;j_B} = Z^{1/2}_{B;\,j_B} b_{B;\,j_B}. \tag{4}$$

As is seen from here and will be demonstrated below, at the fixed available "indirectly determined" values of the ANCs $C_{B;j_B}$ (see, Table 4), variation of single-particle ANC values $b_{B;\,j_B}$ leads to the large uncertainty in the absolute values of the spectroscopic $Z_{B;\,j_B}$. Besides, as a rule, this inaccuracy for $Z_{B;\,j_B}$ can also grow because of optical potentials ambiguities arising

mainly in the interior part of the matrix element. Apparently, the analogous situation may occur for other nucleon transfer reactions induced by a deuteron, including the reactions systematically studied in [34] taking into account the deuteron's break up in the field of the target. In this connection, it should be noted that for small relative distances between colliding light nuclei, which are responsible for the low partial-wave amplitudes corresponding to processes proceeding inside nuclei, the optical model potentials cannot, generally speaking, reflect the true nature of many-particle nuclear interactions [29]. Therefore, the dependence on the single-particle ANCs and optical model potentials in the interior part of the matrix element can be one of the main reasons of the strong dependence of empirical ("experimental") values of the spectroscopic factors $Z_{B;\,j_B}$ extracted from different forms of the DWBA analysis (see, Refs. [20, 24]).

Nevertheless, if the ^{7}Be(d,n)^{8}B reaction is peripheral in the angular region near the main peak the contribution of the internal part into the $\mathcal{R}_{j_B}(E_i,\theta;\,b_{B;\,j_B})$ must strongly be suppressed. In this case, Eq. (2) can be used for determination of the square ANCs $C^2_{B;\,j_B}$, since, in the external part of the matrix element, the optical potential ambiguity and the dependence of the $\mathcal{R}_{j_B}(E_i,\theta;\,b_{B;\,j_B})$ function on $b_{B;\,j_B}$ can be reduced to minimum. To this end, according to [27], at the fixed values of $b_{d;\,1/2}$, λ and optical model parameters for the initial and final states, obviously the peripheral character for the ^{7}Be(d,n)^{8}B reaction is conditioned by

$$\mathcal{R}_{j_B}(E_i,\theta;\,b_{B;\,j_B}) = f(E_i,\theta), \tag{5}$$

where the left-hand side of Eq. (5) should not depend on $b_{B;\,j_B}$ for each fixed energy E_i and scattering angle θ belonging to the main peak region. Then from (2) and (5) the following condition

$$C^2_{B;3/2} = \frac{d\sigma/d\Omega}{\mathcal{R}_{3/2}(E_i,\theta;\,b_{B;3/2}) + \lambda\mathcal{R}_{1/2}(E_i,\theta;\,b_{B;1/2})} = const \tag{6}$$

must be fulfilled for each fixed energy E_i, θ and the function of $\mathcal{R}_{j_B}(E_i,\theta;\,b_{B;\,l_B j_B})$ from (5).

Thus, introduction of the conditions (5) and (6) into the DWBA analysis guarantees the correct absolute normalization of the peripheral reaction cross section and supports the assumption about the dominance of the peripheral character of the proton transfer within (or near) the main peak region of the angular distribution, which is mainly determined by the true peripheral partial-wave amplitudes at $l >> 1$ [19]. Therefore, fulfilment (or weak violation within the errors of the experimental differential cross section $d\sigma^{exp}/d\Omega$) of the conditions (5) and (6) makes it possible to obtain the experimental ("indirectly determined") value of squared ANC $(C^{exp}_{B\,j_B})^2$ for $^7\mathrm{Be}+p\to{}^8$B using the $d\sigma^{exp}/d\Omega$, measured in the main peak of the angular distribution, for $d\sigma/d\Omega$, the values of $C^2_{d;\,1/2}$ [14, 32] and the parameter $b_{d;\,1/2}$ given above in the right hand side (r.h.s.) of (6).

B. Asymptotic normalization coefficients for $^7\mathrm{Be}+p\to{}^8$B

To determine the ANC values for $^7\mathrm{Be}+p\to{}^8$B, the experimental differential cross sections measured in inverse kinematics for the ^{7}Be$(d,n)^8$B reaction at the energy of E_i=4.5 MeV [23] were reanalyzed by the modified DWBA.

Four sets of the optical potentials listed in Table 1 were used. These were obtained from the global parametrization given in [35–39] and a χ^2 minimization analysis by means of the best fits to the experimental $d + {}^7$Li, $n + {}^9$Be and $n + {}^{11}$B scattering angular distributions in the forward hemisphere at the corresponding projectile energies. Such a way of the fitting provides equally good reproduction of the experimental angular distribution within the main peak region as it will be shown below. As an illustration, for the sets 2–4 of the optical potentials, Fig. 1*a* shows the results of comparison between the calculated angular distributions and the experimental data for elastic $d+{}^7$Li scattering taken from Ref.[36] (closed triangles) at most near corresponding energies. As is seen from this figure, the used sets reproduce well the corresponding experimental angular distributions up to $\sim 90^o$. A similar result is obtained for set 1 of Table 1. Besides, in Fig 1*a*, the result of calculation (dash-dotted line), obtained with the optical potentials for the set $S1$ recommended in Ref. [23], and its comparison with the experimental data [23] (open circle) are presented for the elastic $d + {}^7$Be scattering at E_i=4.5 MeV. One can see that the optical potentials recommended in [23] describe well the experimental data only in the narrow angle range of the forward hemisphere. In this connection, we note that the deuteron groups corresponding to the ground and first excited states were not resolved in the experiment. Moreover, a comparison of behavior of the experimental angular distributions of the elastic deuteron scattering on the nuclei ^{7}Be and ^{7}Li shows the overestimation of values of the elastic cross section in the angular range 55–75^o in [23]. It may be the result of the underestimation of the cross section of the inelastic scattering with the formation of the 427 keV excitation level in ^{7}Be in the angle range mentioned above. Indeed, as can be seen from Fig. 5 of Ref. [36], at the elastic deuteron scattering on the nucleus ^{7}Li, the first minimum of the angular distribution is smoothly displaced towards small angles increasing the relative energy (approximately from 80^o at 4 MeV to 70^o at 5 MeV). The value of the differential cross section for the ^{7}Be$(d, d_o)^7$Be data at 4.5 MeV [23] changes by $\sim$2.4 times between the scattering angles 60–75^o (i.e., on the left slope of the expected first minimum of the angular distribution), still not reaching the minimum. Whereas at the same energy (from the data averaged on energy at 4 and 5 MeV [36]), the differential cross section for ^{7}Li$(d, d_o)^7$Li scattering changes only by $\sim$ 1.3 times, reaching the first minimum at an angle $\sim 75^o$. It should be noticed that the position of the first minimum depends very smoothly on the mass number at the fixed energy (see for example, work [39]), therefore the trend of the angular distribution and position of the first minimum for deuteron scattering on ^{7}Li and ^{7}Be nuclei should be similar. For specification of the cross section behavior in the region of the first minimum of angular distribution, which is an essential criterion for the realistic OMP selection, the experiment with a smaller energy dispersion of the ^{7}Be beam is needed. Taking into account the above-stated considerations, we do not include the OMPs recommended in [23] for the analysis of the ^{7}Be$(d, n)^8$B reaction performed below.

For calculation of the shell model two-body bound ^{8}B$(^7\text{Be} + p)$ state wave functions the Woods-Saxon potential is used with varying the geometric parameters within the physically acceptable limit by means of adjusting the well depth to the experimental binding energy (137 keV) for each of the geometric parameters. At first, we have tested validity of the condition (5) for the first six experimental points of the angular distribution of the reaction presented in [23] and for all sets of the optical potentials of Table 1. This test is done by changing the geometric

parameters r_o and a of the Woods-Saxon potential, used for calculation of the bound $(^7\mathrm{Be}+p)$ state wave function, in a wide physically acceptable ranges (r_o=1.10–1.40 fm and a=0.50–0.75 fm) with respect to their "standard" values (r_o=1.25 fm and a=0.65 fm). Such variation of the r_o and a results in changing the single-particle ANCs ($b_{\mathrm{B};\,j_B} = b_{\mathrm{B};\,j_B}(r_o,\,a)$ [25]) with j_B=1/2 and 3/2) within the intervals of $0.615 \leq b_{\mathrm{B};\,3/2} \leq 0.795$ fm$^{-1/2}$ and $0.596 \leq b_{\mathrm{B};\,1/2} \leq 0.782$ fm$^{-1/2}$. The calculations show that over these intervals the condition (5) for each angle θ within the main peak region is fulfilled within $\pm 1.5\%$, whereas $\sigma^{\mathrm{DW}}_{l_d l_B}(E_i, \theta;\, b_{\mathrm{B};j_B})$ entering (3) is a rapidly varying function of $b_{\mathrm{B};\,j_B}$ for j_B=1/2 and 3/2.

Fig. 2 shows a plot of the $\mathcal{R}_{3/2}(E_i, \theta;\, b_{B;\,3/2})$ dependence on the single-particle $b_{\mathrm{B};\,3/2}$ for the potential of the set 3 in Table 1 within the aforementioned interval for three angles θ within the main peak. The width of the band for these curves is the result of the weak "residual" (r_o, a) dependence of $\mathcal{R}_{3/2}(E_i, \theta;\, b_{B;\,3/2})$ on the parameters r_o and a (up to $\pm 1\%$) for $b_{\mathrm{B};\,3/2}(r_o, a)$=const [25]. The same dependence is also observed for j_B=1/2. For example, the arithmetic averaged values of the $\mathcal{R}_{3/2}(E_i, \theta;\, b_{B;\,3/2})$ and $\mathcal{R}_{1/2}(E_i, \theta;\, b_{B;\,1/2})$ obtained in the intervals for $b_{B;\,j_B}$ (j_B=1/2 and 3/2) mentioned above are equal to 49.76 ± 0.04 and 72.31 ± 0.18 mb·fm/sr at $\theta = 16.58^o$ and equal to 25.61 ± 0.01 and 39.41 ± 0.12 mb·fm/sr, respectively, at $\theta = 29.6^o$. Here, the pointed out the uncertainties are the averaged square errors (a.s.e.), which involve those arising due to the observed weak dependence of these calculated functions with changing of $b_{p^7\mathrm{Be};\,j_B}$ and their weak "residual" (r_o, a) dependence of $\mathcal{R}_{3/2}(E_i, \theta;\, b_{B;\,j_B})$ at $b_{B;\,j_B}$=const. It is seen that, at fixed values of θ and E_i the averaged values of the $\mathcal{R}_j(E_i, \theta;\, b_{B;\,j_B})$ functions do not depend practically on the free parameter $b_{B;\,j_B}$. The same situation is observed for the other considered values of θ and the sets of the optical potentials from Table 1.

We also performed calculations of the DWBA cross sections (2) at forward angles for different values of the cutoff radius R_{cut} (lower limit in radial integration over the distance (R) between centers of masses of the colliding particles) to check in an independent manner the peripheral character of the $^7\mathrm{Be}(d,n)^8\mathrm{B}$ reaction at energies E_i=4.5 MeV. Calculations have been done for all sets of the optical potentials of Table 1 and the Woods-Saxon potential for the bound state of ^{8}B with the standard geometric parameters (r_o=1.25 fm and a=0.65 fm) and the Thomas spin-orbital term. The dependence of the DWBA cross sections on the R_{cut}, $\frac{d\sigma}{d\Omega}(R_{cut})$ is shown in Fig. 3a for set 3. It shows that the contribution of the region with $R \leq R_{cut} \lesssim 5.0$ fm into the calculated DWBA cross section is strongly suppressed and practically negligible. The bound state wave functions $r\varphi_{B;\,j_B}(r)$ (j_B=3/2) of the ^{8}B nucleus in the $(^7\mathrm{Be}+p)$-channel calculated for different values of the geometric parameters reach their asymptotic behaviour $b_{B,\,3/2} W_{-\eta_B;3/2}(2\kappa r)$ for $r \gtrsim 5.0$ fm, where $W_{-\eta_B;3/2}(x)$ is the Whitteker function; η_B is the Coulomb parameter for $^8\mathrm{B}=(^7\mathrm{Be}+p)$ bound state and $\kappa = \sqrt{2\mu_{p^7\mathrm{Be}}\varepsilon}$ in which ε is the binding energy of ^{8}B in $(^7\mathrm{Be}+p)$-channel. Fig. 4 demonstrates the dependence of the bound state wave function $r\varphi_{B;\,j_B}(r)$ (j_B=3/2) on the geometric parameters r_o and a of the Woods-Saxon potential.

Testing the condition (5) and calculating the DWBA cross sections (2) at the first four experimental points of the angular distribution also were done for different values of the cutoff radius R_{cut} for the $^7\mathrm{Be}(d,n)^8\mathrm{B}$ reaction at the energy E_i=5.8 MeV [22]. The calculations were performed for the sets 1a, 2a and 3a of the optical potentials obtained by means of fitting experimental scattering data closest to the kinematics of [22] energies in the same way as it is

done above. The results are presented in Table 1. Fig. 1*b* shows the results of comparison of the angular distributions calculated for the sets 1*a* and 2*a* (solid and dashed lines, respectively) with the experimental data for elastic $d + {}^7$Li scattering taken from Ref.[36] (open circles and closed triangles for E_d=7.0 and 8.0 MeV, respectively). As it is seen from the figure, the used sets reproduce well the corresponding experimental angular distributions up to $\sim 90^o$, whereas the optical potentials recommended in [22] provide poor fits to the experimental data (see dash-dotted and dotted lines in Fig. 1*b*). The same situation is observed for set 3*a*. But, the calculations performed for all the considered sets of the optical potentials show that the condition (5) is fulfilled within $\pm 15.0\%$ over the mentioned above intervals for $b_{\mathrm{B};\,3/2}$ and $b_{\mathrm{B};\,1/2}$ for each angle θ within the main peak region. The same situation was observed in [26] where the optical potentials of [22] were used. The dependence of the DWBA cross sections on R_{cut} at the forward angles is shown in Fig. 3*b* for set 1*a*. As is seen from the figure, the contribution of the region with $R \leq R_{cut} \lesssim 5.0$ fm to the calculated DWBA cross section is noticeable and occurs to be about of 30%. The same result is obtained for the sets 2*a* and 3*a*.

It follows from here that the ${}^7\mathrm{Be}(d,n){}^8\mathrm{B}$ reaction at the energy E_i=5.8 MeV is not purely peripheral due to the fact that the contribution of the interior part of the matrix element into the $\mathcal{R}_{3/2}(E_i, \theta;\, b_{B;\,j_B})$ function is significant. One notes once more that the strong dependence of this function on $b_{B;\,j_B}$ is mainly associated with the interior part of the matrix element and is determined by the bound state $\varphi_{B;\,j_B}(r;\, b_{B;\,j_B})$ wave function, which is displayed in Fig. 4 for j_B=3/2 and three fixed values of $b_{B;\,j_B}$ ($b_{B;\,j_B}$=0.620; 0.768 and 0.796 fm$^{-1/2}$). For these values of $b_{B;\,j_B}$ the calculated wave functions change noticeably in the interior region, whereas the observed discrepancy grows from 3% to 8% as the relative distance between the "valence" proton and the center mass of the core (^{7}Be) decreases from 3.0 fm to 0.2 fm (see, the insert in Fig. 4).

Therefore, here in reality one should take into account the effect of a node at short distance in the bound state wave function which is due to Pauli antisymmetrization. Besides, as is mentioned above, the additional difficulty, connected with uncertainties of the optical model potentials in the interior part of the matrix element for description of the elastic scattering of lightest particles on light nuclei [25, 34, 40], can be faced. The facts mentioned above can apparently be one of the reasons why the value of the spectroscopic factor for ^{8}B in the $({}^7\mathrm{Be} + p)$ configuration, extracted in [24] from the ${}^7\mathrm{Be}(d,n){}^8\mathrm{B}$ analysis at the energy E_i=5.8 MeV with using different sets of the input data, has a large spread (about 30%). Therefore, the analysis of the experimental data of [22] performed within the modified DWBA in [26] and in the present work as well as that performed in [24] cannot allow one to obtain the reliable ANC values for astrophysical application. In contrast to this case, as it is demonstrated above, the ${}^7\mathrm{Be}(d,n){}^8\mathrm{B}$ reaction at the energy E_i=4.5 MeV is predominantly peripheral in the main peak region of the angular distribution. At this case, the influence of the effects connected with the true structure of many-particle wave functions of the nuclei (deuteron, ^{7}Be and ^{8}B), exhibited mainly in the interior part of the matrix element, can be ignored. So, in the surface and outer regions of the nucleus, the wave functions of the relative motion at the initial and final states can be described by the optical model, and the bound $[({}^7\mathrm{Be} + p)]$ state wave function by the one-particle shell model wave function in a correct manner reducing their uncertainties to a minimum. Consequently, the experimental data of [23] are used for obtaining the "indirectly

determined" values of the ANCs for $^7\mathrm{Be} + p \to {}^8\mathrm{B}$.

The condition (6) was used for each θ from the main peak region of the angular distribution as only in such a case is the absolute value of the differential cross section defined by the "experimental" value of the ANC. For illustration, we present in Fig. 5 the results of a calculation of the ratio in the r.h.s. of the expression (6), where instead of the calculated differential cross section the corresponding experimental cross sections are taken. The calculations were performed for θ=16.6^o and 29.6^o and the sets 2 and 3 of the optical potentials. Here, it was taken into account the fact that the ratio $\tilde{R} = b_{B;\,1/2}(r_o,\, a)/b_{B;\,3/2}(r_o,\, a)$ does not depend practically on variation of the free r_o and a parameters of the Woods–Saxon potential (r_o ranging from 1.10–1.40 fm and a in the range of 0.50–0.75 fm). The value of $\tilde{R}$ is equal to 0.9742$\pm$0.0065. It is seen from the figure that the C_B^2 values are weakly dependent on the $b_{B;\,3/2}$ value. However, the values of the spectroscopic factor Z_B determined by the relation Z_B=1.006$C_B^2/b_{B;\,3/2}^2$, which can be obtained from (4) and using the aforementioned values for $\tilde{R}$ and λ, change strongly (Fig. 5 (top)). We found that the same dependences for C_B^2 and Z_B occur for all other considered scattering angles and the sets of the optical potentials from Table 1.

To increase the accuracy of the ANC values required for their astrophysical application, the contribution of the compound ($^9\mathrm{B}^*$) nucleus (CN) and coupled channel effects (CCE) connected with the elastic and inelastic $d + {}^7\mathrm{Be}$ scattering should be taken into account, similar as it was done in Refs. [22, 23] and [41, 42]. The influence of the CN contribution Δ_{CN} on the ANC values extracted for each θ from the main peak region has been determined using the results of work [23], where $\Delta_{CN} = 2|d\sigma_{CN}/d\Omega - d\sigma/d\Omega|/(d\sigma_{CN}d\Omega + d\sigma/d\Omega)$ in which $d\sigma_{CN}/d\Omega$ is the CN cross section. The contribution of Δ_{CN} increases with increase of θ in the main peak region what leads to a decrease of the ANC values, obtained from the relation (6). For example, it is by 0.8% at θ=8.2^o and by 2.9% at θ=34.2^o for the set 1 and by 1.0% at θ=8.2^o and by 3.1% at θ=34.2^o for the set 3. The same results practically occur for other sets of the used optical potentials. As a whole the CN contribution to the cross sections [23] in the main peak region is quite small and, consequently, it results in barely changing the extracted ANC values. The CCE contributions to the DWBA cross sections for each experimental point of θ from the main peak region, denoted by Δ_{CCE}=2$|d\sigma_{CCE}/d\Omega - d\sigma/d\Omega|/(d\sigma_{CCE}/d\Omega + d\sigma/d\Omega)$ [41], where $d\sigma_{CCE}/d\Omega$ is the coupling channel cross section, has been determined using the FRESCO computational code [43]. The coupling between the ground (E^*=0.0; J^π=3/2$^-$) and first excited (E^*=0.429 MeV;J^π=1/2$^-$) states of the ^{7}Be nucleus was calculated with the collective form factor of the rotational model for the quadrupole transition, as it was done in [42] (see the coupling scheme in Fig. 6). The spectroscopic amplitudes A_j are taken from Ref. [22] ($A_j = Z_j^{1/2}$). For the core-core interaction the optical potentials adopted for the exit channel of the analyzed reaction are used since there are no optical potentials for the n^7Be-scattering. The deformation length δ_2 is taken equal to 2.0 fm, which results in a change of the deformation parameter $\delta_2(=\beta_2 R_{Be}$, where $R_{Be} = r_o 7^{1/3})$ from 1.02 to 1.04 in a dependence on the parameter radius r_o for the real parts of the used optical potentials. The averaged value of the β_2 is equal to 1.03, which is in a good agreement with the value of 1.00 obtained in [44] from the analysis of $\alpha + {}^7\mathrm{Li}$-scattering. The results are shown in Table 2 where the coupling channel differential cross sections and the coupled channel corrections (percentagewise) are given in the forward hemisphere and all sets of the optical potentials used are shown. As it is seen from Table 2,

for all the used sets of the optical parameters the influence of contribution of the CCE on the ANC values becomes larger as the scattering angle increases. For example, taking into account the CCE contribution increases the ANC values by 2.1% at θ=8.2^o and by 9.4% at θ=34.2^o for the set 1 and decreases the ANC values by 1.0% at θ=8.2^o and by 9.0% at θ=34.2^o for the set 3. Thus, the detailed study of the peripheral character of the considered reaction makes it possible to extract the values of ANCs $C^2_{B;\,3/2}$ and $C^2_{\rm B}[=C^2_{B;\,3/2}(1+\lambda)]$ by using in the r.h.s. of the relation (6) the experimental differential cross sections and values of the function $\mathcal{R}_{j_B}$ for the different scattering angles from the forward hemisphere. At this, the contribution of the compound nucleus and the CCE to the extracted ANC values should be taken into account.

The results of the ANC obtained for each experimental θ point and corresponding to the sets 1–4 are presented in Fig. 7 (a)–(d), respectively. The uncertainties pointed out in this figure correspond to those found from Eq. (6) (a.s.e.), which includes both the experimental errors in the corresponding $d\sigma^{exp}/d\Omega$ and mentioned uncertainties in the $\mathcal{R}_j(E_i,\theta;\,b_{B;\,j})$ functions. The solid line and the width of the band present the results for the weighted mean values and their uncertainties [45], respectively. It is seen from Fig. 6 that the r.h.s. of the relation (6) practically does not depend on the angle θ although absolute values of the experimental cross sections depend noticeably on the angle θ and change by up to the factor 2.6 with θ changing from 8.2^o to 34.2^o.

The weighted mean values of the squared ANCs obtained from all ANC values corresponding to different values of θ in the forward hemisphere are presented in the lines 1–8 of Table 3 for the sets 1–4 of the optical potentials. The uncertainties shown for each set of the optical potentials correspond to the weighted uncertainty, which includes only the experimental errors in the measured differential cross sections. There, the weighted mean values of the squared ANCs extracted without taking into account the CN and CCE contributions are also presented in parenthetical figures. An influence of the CN and CCE contributions on the ANC values is also observed. As is seen from Table 3, the weighted mean value of the ANCs depend weakly on the set of the optical parameters used, and their spread is within the experimental uncertainties for the $d\sigma^{\rm exp}/d\Omega$ [23]. The averaged value of the squared ANCs C^2_B recommended in this work is presented in the ninth and eleventh lines of Table 3 in which the theoretical uncertainty is the a.s.e. connected with the used sets of the optical potentials and the uncertainty in the $\mathcal{R}_{j_B}(E_i,\theta;\,b_{B;\,j_B})$ mentioned above. There the experimental uncertainty is the averaged arithmetic error obtained from the errors for each set of the optical potentials. The overall uncertainties, which are the a.s.e. of the experimental and theoretical ones, are presented in the eleventh and twelfth lines. It is seen from Table 3, the CN and CCE contributions change the ANC values about 4% and the overall uncertainty for the derived ANCs is about 7%, whereas the theoretical and experimental ones are about 3.5% and 6.1%, respectively, i.e., the experimental uncertainty is fairly larger (a factor about 1.7) than the theoretical one. The ANC value recommended in the present work is C^2_B=0.626$\pm$0.022(th)$\pm$0.038(exp) fm^{-1} or C^2_B=0.626$\pm$0.044 fm^{-1} with the overall uncertainty, which are also listed in the second and third lines of Table 4 together with those obtained by the other authors in [10,16,20,24,46–50]. As is seen from Table 4, the weighted mean value of C^2_B, obtained in the present work, is in excellent agreement with that of [10], which was derived from the independent analysis of the experimental ^{7}Be$(p,\gamma)^8$B astrophysical S factors at extremely low energies. However, the

obtained value for C_B^2 differs noticeably from that recommended in [16, 24, 46, 47]. As we discussed above, the ANC value of [16] is model dependent [9, 19, 20, 51] on account of using the first order over the ΔV_f^C potential. The ANC value of [24] and the discussed theoretical uncertainty of it, which can easily be obtained using the $S_{17}(0)$ value derived in [24] (see, Table 4) and its relation with the ANC given there, is also model dependent because of the fairly large ambiguity for the spectroscopic factors. The results of [46] and [47] were obtained from the ^{7}Be$(p,\gamma)^8$B R-matrix analysis, where the direct part of the amplitude is expressed in terms of the channel reduced width and is also determined by a model dependent way. In reality, the ANC value obtained in [46] and [47] can have the uncertainty arising due to an ambiguity in values determined by fitting all the other free parameters used. In addition, as is seen from Table 4, the ANCs obtained by us also differ noticeably from the values of C_B^2 derived in [20, 48] from the ^{208}Pb$(^8\mathrm{B}, \mathrm{p}^7\mathrm{Be})^{208}$Pb breakup reaction. In [20], this process is analysed, as noted above, within the strict three-body model based on the CDCCM in which all nuclear and Coulomb interactions are exactly taken into account in the all-order perturbation theory in the transition operator. Nevertheless, firstly, the cross section of the considered breakup process is expressed in terms of the spectroscopic factor Z_B (denoted by α in [20]), which is really model dependent. Secondly, in [20], the dependence upon channel spin is ignored in the effective p-^{7}Be interaction for the single particle wave function of ^{8}B and the overestimated value of λ(=0.159) was used (see, above and [16, 33]). Therefore, under such assumptions the Z_B value extracted in [20], which was used in Eq. (4) together with the single-particle ANC value for the adopted potential, becomes strongly model dependent. For example, the values of $\omega_I = \sqrt{Z_{B;\,I}/Z_B}$ in terms of which the calculated single particle cross section (σ) is parameterized (see, Eq. (45) in [20]), are taken equal to 0.397 and 0.918 for I=1 and 2, respectively, where I is a channel spin. But, they are equal to 0.497 and 0.868 for I=1 and 2 for Barker's spectroscopic factors ($Z_{B;\,I=1}$=0.251 and $Z_{B;\,I=2}$=0.765) [52]. Apparently, all these facts are the possible reasons why the ANC derived in [20] is underestimated in respect to that obtained in the present work. In [48], the consideration is restricted only by the Coulomb interactions in the first-order perturbation theory in the transition operator. However, as it was demonstrated in [24], this assumption is not correct and leads to the underestimated value of the ANC obtained. Besides, in [48] the three-body Coulomb postdecay acceleration effects in the final state of the Coulomb breakup reaction is not taken into account. As is shown quantitatively in [53], the influence of these effects grows as the relative kinetic energy E of the breakup fragments deceases, especially at extremely low energies. But, our result for ANC obtained for j_B=3/2 is in good agreement with that of [49] derived from the ^{58}Ni$(^8\mathrm{B}, p^7\mathrm{Be})^{58}$Ni analysis for the $1p_{3/2}$ proton orbital in ^{8}B. Besides, the result of [50], obtained within the three-body microscopic approach for the nucleon-nucleon MN potential, is aslo in a good agreement with that of the present work. It follows from here that the microscopic three-body ($\alpha^3\mathrm{He}\,p$) cluster calculation performed in [50] for MN potential correctly reproduces the normalization of the tail of the radial overlap function of the ^{8}B in the ($^7\mathrm{Be}+p$)-channel.

The weighted mean value for C_B^2 presented in Table 3 for the sets 1-4 of the optical potentials and the corresponding central values of the $\mathcal{R}_{j_B}(E_i,\theta;\, b_{B;\,j_B})$ functions were used in the expressions (2) and (3) for calculating the differential cross sections for the ^{7}Be$(d,n)^8$B reaction at E_i=4.5 MeV. The results of calculations and their comparison with the experimental data

[23] are displayed in Fig. 8. As is seen from this figure, the calculated cross section is in a good agreement with the experimental data in the main peak region of the angular distribution for all sets of the optical potentials.

III. APPLICATION FOR THE NUCLEAR ASTROPHYSICAL REACTION AND THE EFFECTIVE-RANGE EXPANSION

C. $S_{17}(E)$ for ^{7}Be$(p,\gamma)^8$B reaction at solar energies

The ANC value for $p+^7\mathrm{Be} \to {}^8\mathrm{B}$ presented in the last line of Table 3 was used for calculation of the astrophysical S factor of the $^7\mathrm{Be}(p,\gamma)^8\mathrm{B}$ reaction at zero energy by using the formula [15]

$$S_{17}(0) = 37.26 C_{\mathrm{B}}^2 \text{ (eVb)}. \tag{7}$$

The obtained value of $S_{17}(0)$ is presented in Table 4 along with the results obtained within the other methods by other authors. As is seen from Table 4, the $S_{17}(0)$ value obtained in the present work is in a good agreement with that of [10] and of [50] obtained for the MN potential as well as with $S_{17}(0)$=23.27 eV b, which can be obtained from the interpolating formula $S_{17}(E)$=23.27-40.53E+327.30E^2 derived by us from the polynomial formula (43) of [54] for Barker's potential and the above mentioned values of the spectroscopic factors [52]. At the same time, our result differs from those of [16, 20, 23, 24, 46, 47, 51, 55, 56]. In this connection, it should be noted the following. In [16, 20, 23, 24, 46, 47] the value $S_{17}(0)$ was obtained by using the underestimated value of the ANC in respect to that derived in the present work. In [20], to obtain the value of $S_{17}(0)$ the relation between $S_{17}(0)/C_B^2$ and the s-wave $^7\mathrm{Be}+p$ scattering length [57] (see, also below) was used in which the scattering lengths for I=1 and 2 were calculated with the Barker's potential. The ANCs were extracted there by using the another form of the p-^{7}Be potential by ignoring its I-dependence, and therefore, these calculations were not self-consistent. In [51, 55, 56], for obtaining the $S_{17}(0)$ value the procedure of the artificial fitting the highly precise experimental data measured there to the astrophysical S factors calculated in [50] was applied. Therefore, the results of [51, 55, 56] obtained for $S_{17}(0)$ are model dependent since the results of [50] presented also in Table 4 appreciably depend on the form of the used NN potentials. The result of the solar fusion II [8], which was complied also from the results of [51, 55, 56], differs also noticeably on that obtained in the present work. Besides, as seen from Table 4, there is the discrepancy between our result for $S_{17}(0)$ and those of [48,58–61] obtained from the ^{8}B Coulomb breakup analysis. Apparently, one of the possible reasons of this discrepancy is the fact that, in [48,58–61], first order over $\Delta V_f^{(C)}$ is used in the transition operator [20] and the mentioned above three-body Coulomb postdecay acceleration effects in the final state [53] are not taken into account. Nevertheless, our result for $S_{17}(0)$ obtained only with taking into account the value of ANC for j_B=3/2, which is equal to 20.6±0.73 eV b, is in excellent agreement with the result of [49]. The latter has also been obtained with taking into account only the $1p_{3/2}$ orbital proton contribution in the ^{8}B nucleus.

The results of extrapolation of the astrophysical S factors at extremely low energies, including close to the Gamov peak, S_{17}(20 keV), S_{17}(50 keV) and S_{17}(120 keV), which can be

obtained within the MTBPA [15] by using the ANC values of the present work, are equal to 22.5±1.8, 21.7±1.8 and 20.8±1.5 eV b, respectively.

We note that the ratio $S_{17}(E)/S_{17}(0)$ obtained from the results of the present work is equal to 0.97, 0.93 and 0.89 at E=20, 50 and 120 keV, respectively. The same results for the ratio can be obtained using the rational expression proposed in [62]. It follows from here that the ratio $S_{17}(E)/S_{17}(0)$ obtained from the results of the present work and that of [62] reproduce correctly the energy dependence of the $S_{17}(E)$ at solar energies ($E \lesssim 120$ keV).

Thus, the C_B^2 value and the values of $S_{17}(E)$ at the solar energies (E=0, 20 and 50 keV) derived in the present work with the uncertainty about 7% confirm the independent results of Ref. [10] obtained with the uncertainty about 3%. Therefore, these can be considered as the "best" values obtained by the indirect method so far. The $S_{17}(E)$ obtained in the present work and in [10] could also be used as the main input data in Eq.(1) for the correct estimation of the solar neutrino flux [1, 8]. Nevertheless, more precise data are need for such estimation of the boron neutrino flux. As it was shown in our paper, the experimental errors dominate in the ANC values extracted from analysis of the ^{7}Be$(d,n)^8$B reaction at 4.5 MeV (c.m.). Moreover, this reaction becomes less peripheral at the larger energies. So, it would be expedient to carry out new precise measurements of the ^{7}Be$(d,n)^8$B reaction and the $d+^7$Be scattering at other near barrier energies of radioactive ^{7}Be (less than 4.5 MeV (c.m.)) and as close to forward scattering angles as possible.

D. s wave $p+^7$Be scattering length and the slop of $S_{17}(0)$

It is now of interest to apply the ANCs and $S_{17}(0)$ derived by us above for obtaining information about experimental values of the s wave $p+^7$Be scattering length $a_o^{(I)}$ and their average one $\bar{a}_o$ [57] (I=1 and 2). To this end, we determine the squared ANC values in other spin coupling modes by using the relation $C^2_{B;\,I} = (C_{B;\,j_B=3/2}+(-1)^I C_{B;\,j_B=1/2})^2/2$ [14] and the averaged values of the $C^2_{B;\,j_B}$ derived in the present work. They are equal to be $C^2_{B;\,I=1}$=0.116±0.014 fm^{-1} and $C^2_{B;\,I=2}$=0.510±0.030 fm^{-1}, which results in $S_{17}^{(I)}(0)/C^2_{B;I}$= 3.685x10^{-5} and 3.727x10^{-5} MeV b fm obtained from (7) for I=1 and 2, respectively. From here and formulas (27) and (28) of [57], we obtain $a_0^{(I)}$ ≈23.2 and 14.8 fm for the s-wave scattering length for I=1 and 2, respectively, as well as the slope of $S_{17}(0)$ near E=0 as $s_1^{(I)} = {S_{17}}^{(I)\prime}(0)/{S_{17}}^{(I)}(0)$ ≈-2.2 and -2.0 MeV^{-1} for I=1 and 2, respectively. Using the values found for the scattering lengths at I=1 and 2 in the formulas (29) and (30) of [57] we can obtain the values of the average scattering length $\bar{a}_o$ and then the value of the slope $s_1 = S'_{17}(0)/S_{17}(0)$. They are equal to be $\bar{a}_o$ ≈16.3 fm and s_1 ≈-2.1 MeV^{-1}. These results for $s_1^{(I)}$ and s_1 are close to those of $s_1^{(1)}$=-1.65 MeV^{-1}, $s_1^{(1)}$=-1.77 MeV^{-1} and s_1=-1.74 MeV^{-1}, which can be obtained from the above mentioned polynomial approximation, as well as to those of s_1=-1.86, -1.92 and -1. 97 MeV^{-1} for the MN and V2 potentials [63], respectively. The slope of $S_{17}(0)$ near E=0 determined in the present work becomes slightly steeper than that predicted in [57, 63]. But, as is seen from here, the s_1 values of [57, 63] depend noticeably on the input potential. The values of $a_0^{(I)}$ (I=1 and 2) and $\bar{a}_o$ obtained in the present work differ significantly from those derived in [20, 57, 64]. In this connection, we note that the magnitudes of $a_0^{(I)}$ and $\bar{a}_o$ defined from the corresponding

expressions of [57] are very sensitive to those of the ratios $S_{17}^{(I)}(0)/C_{B;\,I}^2$ and $S_{17}(0)/C_B^2$, where $S_{17}(0) = \sum_{I=1,2} S_{17}^{(I)}(0) = \sum_{j_B=1/2,3/2} S_{17}^{(j_B)}(0)$ and $C_B^2 = \sum_{I=1,2} C_{B;\,I}^2$. The calculations showed that a small change of the ratios results in considerable change for $a_0^{(I)}$ and $\bar{a}_o$. For example, the values of $a_0^{(I)}$=25 and -8 fm at I=1 and 2 as well as of $\bar{a}_o$=-2.8 fm obtained in [20] give the values of $S_{17}^{(I)}(0)/C_{B;\,I}^2$=3.677x$10^{-5}$ and 3.840x10^{-5} MeV b fm for I=1 and 2, respectively, and $S_{17}(0)/C_B^2$=3.813x10^{-5} MeV b fm. The similar situation occurs in other works mentioned above.

It follows from here that one of the main reasons of the observed discrepancy between the results of the present work and other works for the s-wave $p + {}^7$Be scattering lengths and the slope of $S_{17}(E)$ near E=0 is the deference between the values of the ANCs and $S_{17}(0)$ derived by other authors and those obtained in the present work. From our point of view, our results for the s-wave $p + {}^7$Be scattering lengths and the slope of $S_{17}(E)$ near E=0 are more trustable because they are derived with the minimum ambiguity connected with the ANC and $S_{17}(0)$ values.

IV. CONCLUSION

This scrupulous analysis of the ^{7}Be(d,n)^{8}B reaction data at E_i=4.5 and 5.8 MeV is performed within the modified DWBA. It is demonstrated that the peripheral character of this reaction in the main peak region of the angular distributions occurs only for E_i=4.5 MeV [23]. Therefore, the experimental differential cross sections of the reaction under consideration measured in [23] can be used as a source of determination of the squared ANC values C_B^2 for $p + {}^7\mathrm{Be} \to {}^8\mathrm{B}$. A new value for the ANC was obtained, which is in an agreement with that recommended in [10, 49] and differs strongly from the value, which is deduced within the modified DWBA in [16] from the analysis of the other proton transfer reactions.

The value of the ANC from this work was used for estimation of the astrophysical S factor at E=0 and the value of $S_{17}(0)$ equal to 23.32±1.64 eVb was obtained, which is in excellent agreement with that recommended in [10]. It differs noticeably from that recommended in Refs . [8, 16, 23, 46, 47, 51, 56] and obtained by other authors from the data of the $A(^8B, p^7Be)A$ Coulomb breakup reaction. Also, the new estimation is obtained for the s-wave scattering length for the $p + {}^7$Be scattering and the slope of $S_{17}(0)$ near E=0.

ACKNOWLEDGMENTS

The authors are deeply grateful to L. D. Blokhintsev, K. Ogata and R. J. Peterson for careful reading of the manuscript, discussions and constructive suggestions. The work has been supported in part by the Academy of Sciences of the Republic of Uzbekistan (grants No. F2-FA-F117 and F2-FA-F114).

References

[1] J. N. Bahcall, N. A. Bahcall, R. K. Ulrich, Astrophys. J., **156**, 559 (1969).

[2] J. N. Bahcall, A. M. Serenelli, and S. Basu, Astrophys. J. **621**, L85 (2005).

[3] J. N. Bahcall, W.F. Huebner, S. H. Lubow, P. D. Parker, and R. K. Ulrich, Rev.Mod.Phys. **54**, 767 (1982).

[4] J.N. Bahcall, R.K.Ulrich, Rev.Mod.Phys.**60**, 297 (1988).

[5] J. N. Bahcall, and M. H. Pinsonneault, Rev.Mod.Phys. **64**, 781 (1992).

[6] J. N. Bahcall, S. Basu, and M. H. Pinsonneault, Phys.Lett. **B 433**, 1 (1998); Astrophys. J., **555**, 990 (2001)

[7] C. Rolfs and W.S. Rodney, Cauldrons in the Cosmos,(University of Chicago Press,Chicago and London 1988).

[8] E.G. Adelberger, *et al.*, Rev. Mod. Phys. **83**, 195 (2011).

[9] R. Yarmukhamedov and Q. I. Tursunmahatov. In the book: The Universe Evolution: Astrophysical and nuclear aspects. Nova publishers, New York,USA. Chapter 6, 2013, pp. 219-270.

[10] S.B. Igamov and R. Yarmukhamedov, Phys. At. Nucl. **71**, 1740 (2008).

[11] N.K. Timofeyuk, D. Baye, and P. Descouvemont, Nucl.Phys. A **620**, 29 (1997).

[12] N.K. Timofeyuk, Nucl. Phys. A **632**, 19 (1998).

[13] P. Descouvemont, Phys. Rev. C **70**, 065802 (2004).

[14] L.D. Blokhintsev, I.Borbely, E.I. Dolinskii, Fiz.Elem.Chastits At. Yadra. **8**, 1189 (1977)[Sov. J. Part. Nucl. **8**, 485 (1977)].

[15] S.B. Igamov, and R. Yarmukhamedov, Nucl.Phys.A **781**, 247 (2007);A **832**, 346 (2010).

[16] G. Tabacaru, A. Azhari, J. Brinkley, *et al.*, Phys. Rev. C **73**, 025808 (2006).

[17] A. Azhari, V. Burjan, F. Carstoiu, et al.Phys.Rev.Lett. **82** (1999) 3960.

[18] A. Azhari, V. Burjan, F. Carstoiu, et al.Phys.Rev.C **60** (1999) 055803.

[19] S.B. Igamov, M.C. Nadyrbekov and R. Yarmukhamedov, Phys.At.Nucl.**70**, 1694 (2007).

[20] K. Ogata, S. Hashimoto, Y. Iseri, M. Kamimura, M. Yahiro, Phys.Rev. C **73**, 024605 (2006).

[21] A.R. Junghans, M.C. Mohrmann, K.A. Snover *et al.*, Phys. Rev. C **68**, 065803 (2003).

[22] Weiping Liu, *et al.*, Phys.Rev.Lett. **77**, 611 (1996).

[23] J. J. Das, *et al.*, Phys.Rev.C **73**, 015808 (2006).

[24] K. Ogata, M. Yahiro, Y. Iseri, M. Kamimura. Phys. Rev. C **67**, 011602(R) (2003).

[25] S. A. Goncharov, J. Dobesh, E. I. Dolinskii, A. M. Mukhamedzhanov and J. Cejpek. Yad. Fiz. **35**, 662 (1982) [Sov. J. Nucl. Phys. **35**, 383 (1982)].

[26] O. R. Tojiboev, R. Yarmukhamedov, S. V. Artemov, M. Kajumov. Uzb.J.Phys. **16**, 247 (2014).

[27] I. R. Gulamov, A. M. Mukhamedzhanov, G. K. Nie, Yad. Fiz. **58**, 1789 (1995).

[28] S.V. Artemov, I.R. Gulamov, E.A. Zaparov *et al.*, Yad. Fiz. **59**, 454 (1996)[Phys. Atom. Nucl. **59** , 428 (1996)].

[29] A.M.Mukhamedzhanov, H.L. Clark, C.A. Gagliardi *et al.*, Phys. Rev. C **56**, 1302 (1997).

[30] N. Austern, R. M. Drisko, E. C. Halbert, G. R. Satchler, Phys.Rev. **133**, B3 (1966).

[31] R. M. DeVries, Ph.D. thesis, Ubiversity of California, 1971,. J. Perrenoud and R. M. DeVries, Phys.Lett.B **36**, 18 (1971).

[32] A. M. Mukhamedzhanov, I. Borbely, *at al.*, Izv. AN SSSR, Physics, **48**, 350 (1984).

[33] L. Trache, A. Azhari, F. Carstoiu, *et al.*, Phys.Rev.C **67**, 062801(R), (2003)

[34] X. D. Liu, M. A. Famiano, W. G. Lynch, M. B. Tsang, J. A. Tostevin, Phys. Rev. C **69**, 064313 (2004).

[35] H. Lüdecke, Tan Wan-Tjin, Nucl. Phys. A **109**, 676 (1968).

[36] M. Avrigeanu, W. von Oertson, U. Fischer, V. Avrigeanu, Nucl. Phys. A **759**, 327 (2005).

[37] C. M. Perey, F. G. Perey, Atomic Data and Nucl. Data Tables, **17**, 1 (1976).

[38] P. Pereslavtsev, U. U. Fischer, S. Simakov, M. Avrigeanu, Nucl. Inst. and Merthods in Physics Research B **266**, 3501 (2008).

[39] W. Fitz, R Jahr and R. Santo. Nucl. Phys. A **101**, 449 (1967).

[40] J. P. Schiffer, G. C. Morrison, R. N. Siemsson, B. Zeidman, Phys.Rev. **164**, 1274 (1967).

[41] F. M. Nunes, A. M. Mukhamedzhanov, Phys. Rev.C **64**, 062801(R) (2001).

[42] N. Burtebaev, J. T. Burtebaeva, N. V. Glushchenko, Zh. K. Kerimkulov, A. Amar, M. Nassurulla, S. B. Sakuta, S. V. Artemov, S. B. Igamov, A. A. Karakhodzhaev, K. Rusek, S. Kliczewski, Nucl. Phys. A **909**, 20 (2013).

[43] I. J. Thompson FRESCO, Department of Physics, University of Surrey, July 2006, Guildford GU2 7XH, England, version FRESCO 2.0, http://www.fresco.org.uk/.

[44] N. Burtebaev, A. Duisebaev, B. A. Duisebaev, G. I. Ivanov, S. B. Sakuta, Yad. Fiz.,**59**, 33 (1996)[Phys.Atom.Nucl.**59**, 29 (1996)].

[45] C. Angulo, M. Arnould, M. Rayet, *et al.*, Nucl.Phys.A **656** (1999) 3.

[46] J. T. Huang, C. A. Bertulani, V. Guimarães, Atomic Data and Nuclear Data Tables. **96**, 824 (2010).

[47] F.C. Barker, Nucl.Phys.A **588**, 693 (1995).

[48] L. Trache, F. Carstoiu, C. A. Gagliardi, R. E. Tribble, Phys.Rev.Lett. **87**, 271102 (2001).

[49] T. L. Belyaeva, E. F. Aguilera, E. Martinez-Quiroz, *et al.*, Phys.Rev.C **80**, 064617 (2009).

[50] P. Descouvemont, Phys.Rev.C **70**, 065802 (2004).

[51] L. T. Baby, C. Bordeanu, G. Goldring, *et al.*, Phys.Rev.Lett. **90**, 022503 (2003);Phys.Rev.C **67**, 065805 (2002).

[52] F. C. Barker, Aust. J. Phys. **33**, 177 (1980); Phys.Rev.C **28**, 1407 (1983).

[53] B. F. Irgaziev, A. M. Mukhamedzhanov, Phys.Rev.C **71**, 024602 (2003).

[54] D. Baye, E. Brain, Phys.Rev.C **61**, 025801 (2000).

[55] L. T. Baby, C. Bordeanu, G. Goldring, M. Hass, L. Weissman, V. N. Fedoseyev, U. Köster, Y. Nir-El, G. Haquin, H. W. Gäggeler, R. Weinreich, and the ISOLDE Collaboration, Phys.Rev.C **67**, 065805 (2003).

[56] A. R. Junghans, E. C. Mohrmann, K. A. Snover, T. D. Steiger, E. G. Adelberger, J. M. Casandjian, H. E. Swanson, L. Buchmann, S. H. Park, A. Zyuzin, A. M. Laird, Phys.Rev.C **68**, 065803 (2003).

[57] D. Baye, Phys.Rev.C **62**, 065803 (2000).

[58] N. Iwasa, F. Boué, G. Surówka, *et al.*, Phys.Rev.Lett. **83**, 2910, (1999).

[59] P. Schümann, F. Hammache, S. Typel, *et al.*, Phys.Rev.Lett. **90**, 232501 (2003).

[60] D. Davids, S. Typel, Phys.Rev.C **68**, 045802 (2003).

[61] P. Schümann, S. Typel, F. Hammache, *et al.*, Phys.Rev.C **73**, 015806 (2006).

[62] B. K. Jennings, S. Karataglidis, T. D. Shoppa, Phys.Rev.C **58**, 3711 (1998).

[63] F. C. Barker, Nucl.Phys.A **768**, 241 (2006).

[64] C. Angulo, M. Azzouz, P. Descouvemont, *et al.*, Nucl.Phys.A **716**, 211 (2003).

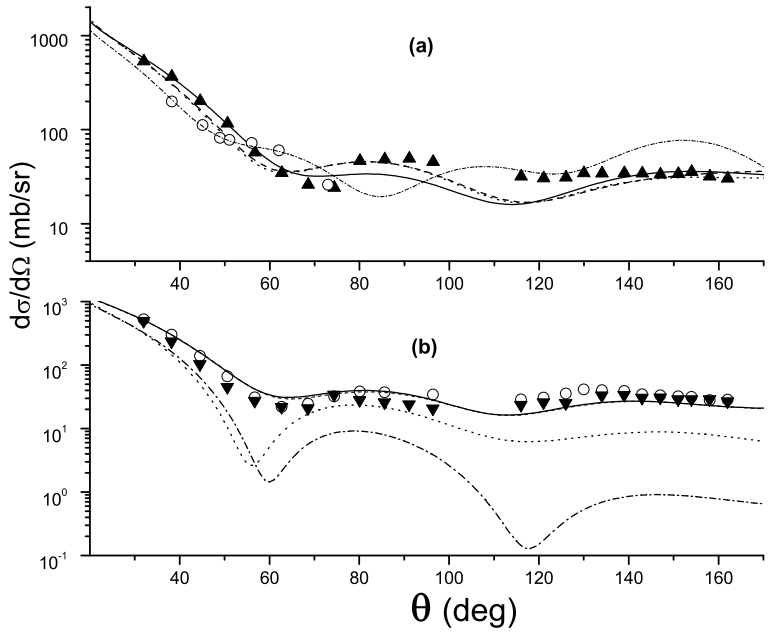

Figure 1: The fit of the elastic $d + {}^7\mathrm{Li}$ and $d + {}^7\mathrm{Be}$ scattering cross sections by using different sets of optical potentials. In (a), the solid, dashed and dotted lines correspond to the sets 4, 3 and 2, whereas the dash-dotted line corresponds to the set S1 from [23]; experimental data for the elastic $d + {}^7\mathrm{Li}$ scattering at E_d=6 MeV (closed triangles) and for the $d + {}^7\mathrm{Be}$ scattering E_d=5.79 MeV (open circles) are taken from [36] and [23], respectively. In (b), the solid and dashed lines correspond to the sets 1a and 2a of the present work, and the dash-dotted and dotted lines correspond to the sets 1 and 2 recommended in [22]; experimental data (open and close points) for the elastic $d + {}^7\mathrm{Li}$ scattering [36] at E_d=7.0 and 8.0 MeV, respectively.

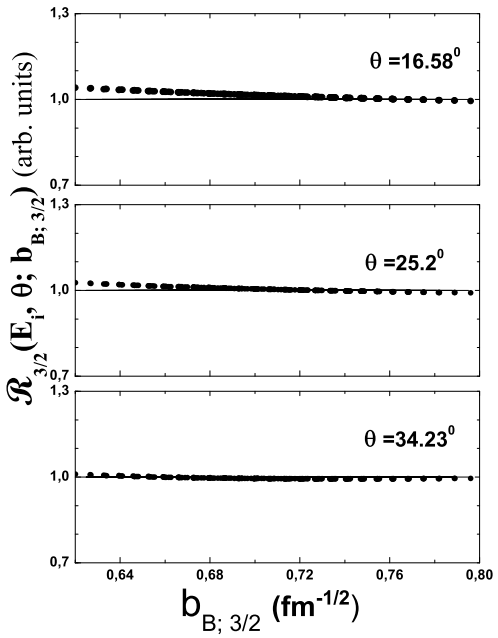

Figure 2: The dependence of $\mathcal{R}_{3/2}(E_i, \theta;\, b_{B;3/2})$ on the single-particle $b_{B;3/2}$ at the different angles θ for the energy of E_i=4.5 MeV and with potential parameters of the set 3 in Table 1. The width of the bands for fixed values of $b_{B;3/2}$ corresponds to variation of the parameters r_o and a of the adopted Woods-Saxon potential within the intervals from r_o=1.10 to 1.40 fm and a=0.50 to 0.75 fm.

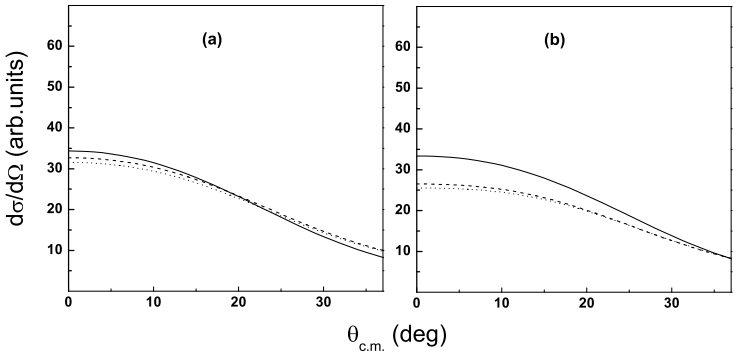

Figure 3: Angular distributions at different cutoff radii (R_{cut}) for E_i=4.5 MeV (a) and E_i=5.8 MeV (b) calculated in DWBA with potential parameters of the sets 3 and 1a (Table 1), respectively. The solid, dotted and dashed lines are the differential cross sections calculated for the cutoff radius R_{cut}=0.0, 4.0 and 5.0 fm, respectively.

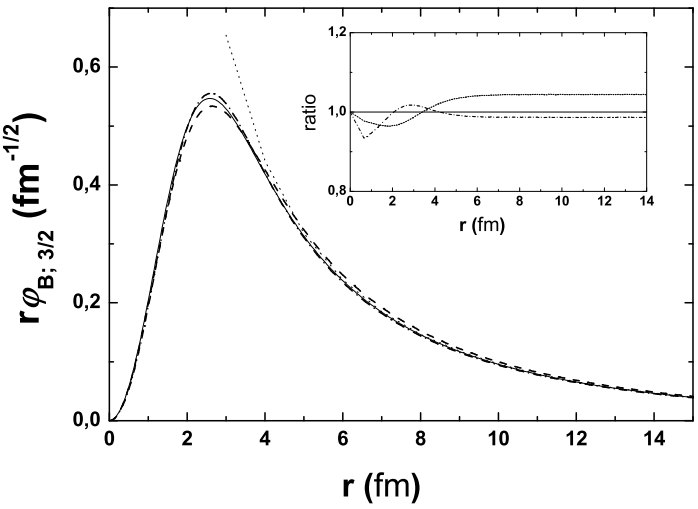

Figure 4: The radial behaviour of the single-particle ^{8}B[=(^{7}Be + p)] bound state wave function $r\varphi_{B;\,j_B}(r)$ with j_B=3/2 calculated for the Woods-Saxon potential with different sets of (r_o, a)-pair and $b_{B,\,3/2}$:(1.00 fm; 0.50 fm) and 0.6200 fm$^{-1/2}$ (the dashed line),(1.25 fm; 0.65 fm) and 0.7679 fm$^{-1/2}$ (the solid line), (1.40 fm; 0.80 fm) and 0.7960 fm$^{-1/2}$ (the dashed-dotted line). The Coulomb radius r_C=1.30 fm. The dotted line is the tail $b_{B,\,3/2}W_{-\eta_B;3/2}(2\kappa r)$ of the bound state wave function $r\varphi_{l_B j_B}(r)$ with $b_{B,\,3/2}$=0.7679 fm$^{-1/2}$(r_o=1.25 fm and a=0.65 fm).

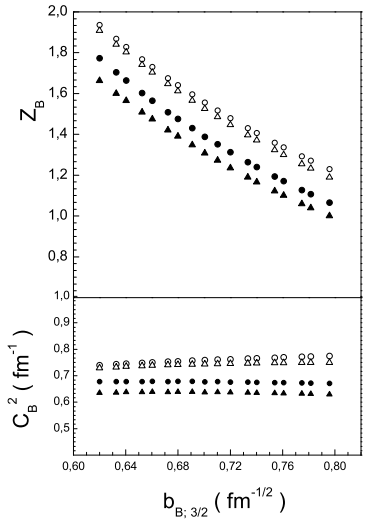

Figure 5: Values of the spectroscopic factors Z_B (top) and the squared ANC C_B^2 (bottom) as a function of the single-particle $b_{B;\,3/2}$ obtained from the modified DWBA ^{7}Be$(d,n)^8$B analysis at the energy E_i=4.5 MeV for the different fixed angles θ and the sets of the optical potentials. Data denoted by $\circ$ and $\triangle$ ($\bullet$ and $\blacktriangle$) correspond to the experimental points θ of 16.6^o and 29.6^o, respectively, for set 3(2).

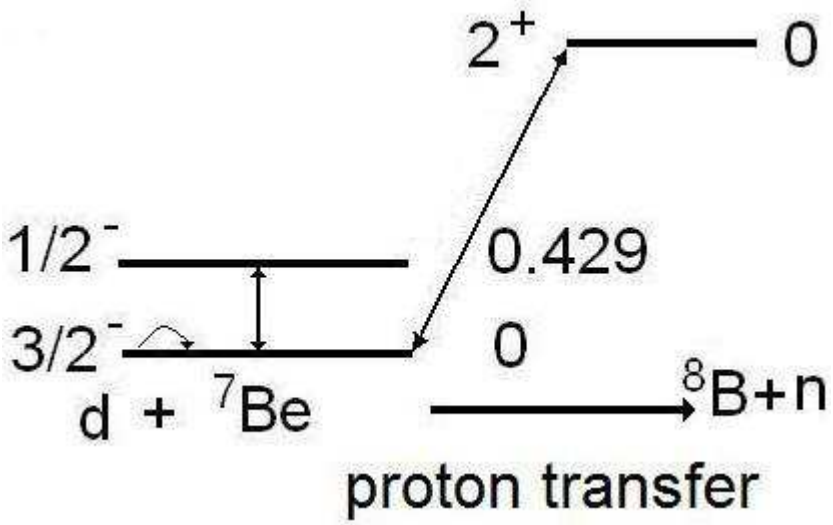

Figure 6: The coupling scheme used in calculations of the cross section for the ^{7}Be$(d,n)^7$Be reaction by the coupled reaction channels method.

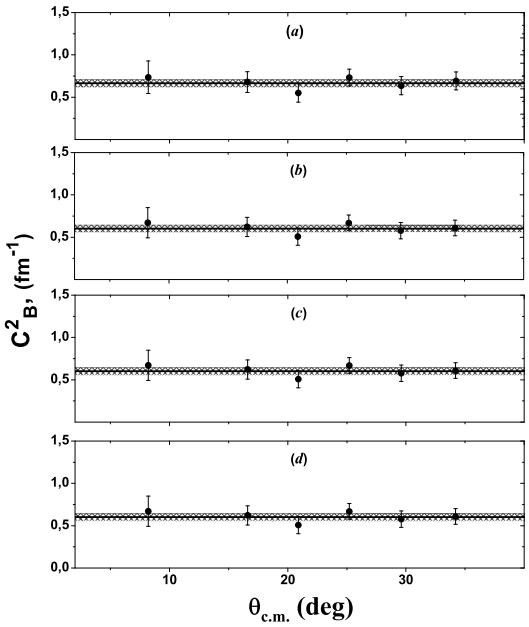

Figure 7: The values of the squared ANC C_B^2 for $^7\mathrm{Be} + p \to {}^8\mathrm{B}$ for each of the experimental θ. Data in (a)–(d) are obtained from the analysis of the experimental differential cross sections of Refs. [23] at E_i=4.5 MeV and the sets 1–4 of the optical potentials, respectively. The solid lines present the results for the weighed mean values. The widths of the bands are the corresponding weighed uncertainties.

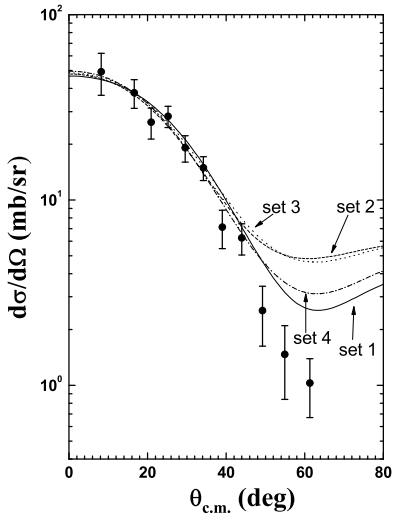

Figure 8: Angular distribution of the differential cross section for the ^{7}Be$(d,n)^8$B reaction at E_i=4.5 MeV together with the theoretical calculations performed for the different sets of the optical parameters from Table 1 using the corresponding weighted mean of the ANC value from Table 2. The experimental data are taken from Ref. [23].

Table 1: Parameters of the optical potentials corresponding to the entrance (a) and exit (b) channels for the ^{7}Be(d,n)^{8}B reaction at the energies E_d=5.79 and 7.46 MeV in the laboratory system.

E_d, (MeV)	set	channel	V, (MeV)	r_V, (fm)	a_V, (fm)	$4W_D(W)$, (MeV)	$r_D(r_W)$, (fm)	$a_D(a_W)$, (fm)	V_{so}, (MeV)	r_{so}, (fm)	a_{so}, (fm)
5.79	1	a	72.0	1.05	0.95	(30.00)	(0.84)	(0.85)	12.8	1.05	0.94
		b	28.0	1.64	1.05	121.2	1.94	0.11	4.9	1.64	0.27
	2	a	67.0	1.35	0.93	18.00	2.48	0.30	16.0	0.86	0.25
		b	47.1	1.31	0.66	33.52	1.26	0.48			
	3	a	66.2	1.35	0.93	17.43	2.43	0.30	16.0	0.86	0.25
		b	35.8	1.51	0.43	25.98	1.84	0.51	5.8	1.18	0.51
	4	a	64.0	1.35	0.90	18.68	2.37	0.30	12.0	0.86	0.25
		b	35.8	1.51	0.43	25.98	1.84	0.51	5.8	1.18	0.51
7.46	1a	a	65.0	1.35	0.89	19.16	2.34	0.30	12.0	0.86	0.25
		b	48.19	1.20	0.72	30.32	1.43	0.66	5.2	1.13	0.77
	2a	a	64.0	1.35	0.90	18.68	2.37	0.30	12.0	0.86	0.25
		b	48.2	1.13	0.72	45.32	1.43	0.66	6.2	1.13	0.77
	3a	a	64.0	1.35	0.90	18.68	2.37	0.30	12.0	0.86	0.25
		b	42.4	1.35	0.55	37.56	1.35	0.75	5.0	1.35	0.55

Table 2: Coupling channel effects for the ^{7}Be(d,n)^{8}B reaction at E_i=4.5 MeV in the forward hemisphere calculated for each set of the optical potential used. Differential cross sections and Δ_{CCE} are given in mb/sr and percentagewise, respectively.

θ,	$d\sigma_{CCE}/d\Omega$ (Δ_{CCE})			
(deg.)	set 1	set 2	set 3	set 4
0.00	45.2(2.7)	34.96(2.9)	33.33(0.3)	34.60(1.1)
8.20	44.6(3.2)	34.25(1.0)	32.60(1.0)	33.99(0.5)
16.60	41.9(4.4)	31.30(1.0)	29.80(3.1)	31.51(1.3)
20.90	39.2(5.5)	28.71(2.7)	27.38(6.4)	29.18(2.6)
25.20	36.6(6.6)	25.80(4.3)	24.60(6.4)	26.47(4.0)
29.60	26.4(9.9)	21.97(6.5)	20.90(8.5)	22.80(5.8)
34.20	26.4(9.9)	17.85(8.8)	17.01(10.7)	18.84(7.7)

Table 3: The dependence of the weighted mean values of the squared ANCs for $^7\mathrm{Be}+p\to{}^8$B from each of the sets 1–4 of the optical potentials at E_i=4.5 MeV. Parenthetical figures are the weighted mean values of the squared ANCs extracted without taking into account the CN and CCE contributions.

set	$C^2_{B;3/2}$, fm^{-1}	C^2_B, fm^{-1}
1	0.590±0.036	0.664±0.040
	(0.563±0.034)	(0.633±0.039)
2	0.514±0.031	0.578±0.035
	(0.551±0.034)	(0.619±0.038)
3	0.587±0.035	0.660±0.039
	(0.641±0.038)	(0.721±0.042)
4	0.536±0.033	0.603±0.037
	(0.569±0.035)	(0.640±0.040)
averaged value	0.557±0.020(th)±0.034(exp)	0.626±0.022(th)±0.038(exp)
	(0.581±0.021(th))±0.035(exp)	(0.653±0.024(theor)±0.032(exp))
	0.557±0.039	0.626±0.044
	(0.587±0.041)	(0.653±0.046)

Table 4: The squared ANC ($C_B^2 = C_{B;\,1/2}^2 + C_{B;\,3/2}^2$) for $^7\mathrm{Be} + p \rightarrow\ ^8\mathrm{B}$ and the astrophysical S factor ($S_{17}(0)$) for the direct radiative capture $^7\mathrm{Be}(p,\gamma)^8\mathrm{B}$ reaction.

Method	$C_B^2(\mathrm{fm}^{-1})$	$S_{17}(0)$(eV·b)	Refs.
MDWBA			the
$^7\mathrm{Be}(d,n)^8\mathrm{B}$	0.626±0.022(th)±0.038(exp)	23.32±0.82(th)±1.42(exp)	present
	0.626±0.044[1)]	23.32±1.64[1)]	work
MTBPA			
$^7\mathrm{Be}(p,\gamma)^8\mathrm{B}$	0.628±0.017	23.40±0.63	[10]
MDWBA			
$^{10}\mathrm{B}(^7\mathrm{Be},^8\mathrm{B})^9\mathrm{Be}$			
$^{14}\mathrm{N}(^7\mathrm{Be},^8\mathrm{B})^{13}\mathrm{C}$	0.465±0.041	18.2±1.8	[16]
Breakup			
$^{208}\mathrm{Pb}(^8\mathrm{B},p^7\mathrm{Be})^{208}\mathrm{Pb}$	0.548	$21.7^{+0.37}_{-0.24}$(th)±0.50(exp)	[20]
CDCCM			
$^7\mathrm{Be}(d,n)^8\mathrm{B}$	$0.545^{+0.036}_{-0.034}$(th)±0.070(exp)	$20.96^{+1.4}_{-1.3}$(th)±2.7(exp)	[24]
R-matrix			
$^7\mathrm{Be}(p,\gamma)^8\mathrm{B}$	0.518[2)]	19.4[2)]	[46]
	0.491	17.3±3.0	[47]
Coulomb breakup			
$\mathrm{A}(^8\mathrm{B},p^7\mathrm{Be})\mathrm{A}$	0.450±0.072	17.4±1.5	[48]
$^{58}\mathrm{Ni}(^8\mathrm{B},\mathrm{p}^7\mathrm{Be})^{58}\mathrm{Ni}$	0.547±0.027[2)]	20.8±1.1[2)]	[49]
microscopic three-	0.812	29.45[3)]	[50]
body ($\alpha^3\mathrm{He}p$) model	0.668	24.65[4)]	[50]
CDCCM DWBA			
$^7\mathrm{Be}(d,n)^8\mathrm{B}$		20.7±2.4	[23]
phenomenological		21.2±0.7	[51, 55]
way		21.4±0.6(th)±0.5(exp)	[56]
Coulomb breakup			
$^{208}\mathrm{Pb}(^8\mathrm{B},p^7\mathrm{Be})^{208}\mathrm{Pb}$		20.6±1.2[5)]±1.0[6)]	[58]
		18.6±1.2[5)]±1.0[6)]	[59, 60]
		20.6±0.8[7)]±1.2[8)]	[61]
solar fusion II		20.8±0.7[5)]± 1.4[6)]	[8]

[1)] the overall uncertainty; [2)] for the $p_{3/2}$ state; [3)]the V2 potential; [4)]the MN potential; [5)]the exp. error; [6)]the th. error; [7)] the stat. error; [8)]the sys.error.